Journal of Alloys and Compounds 509 (2011) 2753–2757

Contents lists available at ScienceDirect

Journal of Alloys and Compounds

journal homepage: www.elsevier.com/locate/jallcom

# Structure, dielectric and electric properties of $(Ba_{0.68-x}Sr_{0.308}Bi_{0.006}Na_{0.006}Mg_x)(Ti_{0.99}Sn_{0.01})O_3$ ceramics

Shiguo Xu*, Yuanfang Qu, Dean Yang

*Key Laboratory for Advanced Ceramics and Machining Technology of Ministry of Education, College of Materials Science & Engineering, Tianjin University, Tianjin 300072, China*

ARTICLE INFO

*Article history:*
Received 2 October 2010
Received in revised form 2 November 2010
Accepted 10 November 2010
Available online 26 November 2010

*Keywords:*
Ceramics
Crystal structure
Dielectric properties
Phase transitions
Conduction

ABSTRACT

$(Ba_{0.68-x}Sr_{0.308}Bi_{0.006}Na_{0.006}Mg_x)(Ti_{0.99}Sn_{0.01})O_3$ ceramics were synthesized by solid-state reaction process. The samples ($X \leq 0.010$) are a mixture of cubic (major) and rhombohedral (minor) phases. The rhombohedral phase causes a large dielectric loss in low temperature regions and plays an important role in diffuse phase transition of ceramics. While $X > 0.010$, the rhombohedral phase decreases and gradually disappears. The dielectric loss of ceramics in the low temperature regions decreases, and the samples change from the diffuse phase transition to the phase transition of second order, and then to of first order. In the temperature range of 270–370 °C, intrinsic conduction dominates conductivity of ceramics.



## 1. Introduction

The dielectric and ferroelectric materials have been widely employed in several industrial applications, such as dynamic random access memory, microwave filters, voltage controlled oscillators and telecommunication technologies [1–4]. The conventional dielectric and ferroelectric ceramics materials were lead oxide ferroelectrics and had outstanding properties. However, the toxicity of lead oxide has been considered to be a serious threat to the environment [5]. Therefore, in the last few years, there has been a strong demand to develop lead-free ceramics, whose dielectric properties should be comparable to those of their lead-containing counterparts.

The researchers paid more attention to improve the dielectric properties of pure $BaTiO_3$ via partial substitution of either Ba-ions (A-site doping) or Ti-ions (B-site doping), which may result to the high permittivity of ferroelectric $BaTiO_3$ ceramics [6]. So far, many new solid solutions with excellent properties have been developed, such as $Ba_{1-x}Sr_xTiO_3$ [7], $BaTi_{1-x}Sn_xO_3$ [8–10] and $(BaSr)(SnTi)O_3$ [11,12] ceramics. Among them, the stannum-containing titanate ceramics (TS), which were prepared by substitution of $Sn^{4+}$ for $Ti^{4+}$ in the ferroelectric lattice, may be considered capacitor ceramics for replacing the lead-containing ceramic because they exhibited the favorable dielectric properties [9–10,13–17].

$(Bi_{0.5}Na_{0.5})TiO_3$ is a complex rhombohedral perovskite which is known for its relaxor ferroelectric features. To the best of our knowledge, few works in the literature have been reported on the doping modification of solid solutions between $(Bi_{0.5}Na_{0.5})TiO_3$ and $(BaSr)(SnTi)O_3$. In this paper, $(Ba_{0.68}Sr_{0.32})(Ti_{0.99}Sn_{0.01})O_3$ ceramic and $(Ba_{0.68-x}Sr_{0.308}Bi_{0.006}Na_{0.006}Mg_x)(Ti_{0.99}Sn_{0.01})O_3$ ceramics were prepared by conventional solid state reaction method. Then phase constitution, dielectric and electric properties of as-synthesized specimens were studied.

## 2. Experimental

The nominal chemical compositions of the specimens were shown in Table 1. The high purity $TiO_2$ (>98.0%), $BaCO_3$ (>99.0%), $SrCO_3$ (>99.0%), $SnO_2$ (>99.0%), $Bi_2O_3$ (>98.0%), $Na_2CO_3$ (>99.8%) and $(MgCO_3)_4{\cdot}Mg(OH)_2{\cdot}5H_2O$ (>99.0%) were used as starting raw materials. After the ball-milling, the mixed raw materials were dried and then calcined at 1080 °C for 2 h. All the calcined powders were mixed with 0.2 at.% ZnO and 0.2 at.% $MnO_2$, reground, dried, granulated (with polyvinyl alcohol as a binder for granulation), pressed into the desired form ($\Phi \times d = 15.00\,mm \times 2.00\,mm$) at 170 MPa, and then the B6M0–B6M30 sintered at 1290–1340 °C for 2 h in the air. The silver paste was painted on both sides as electrodes for dielectric property measurements after the sintered samples were ultrasonically cleaned in distilled water. Finally the painted samples were fired at 850 °C for 20 min.

The capacitance quantity ($C$) and loss factor ($D$) were measured using a capacitance apparatus (Automatic LCR Meter 4225, China) at 1 kHz. The dielectric constant ($\varepsilon_r$) and dielectric loss tangent ($\tan\delta$) were calculated as follows:

$$\varepsilon_r = \frac{14.4Ch}{\phi^2} \quad (1)$$

* Corresponding author at: Key Laboratory for Advanced Ceramics and Machining Technology of Ministry of Education, College of Materials Science & Engineering, No. 92, Weijin Road, Tianjin University, Tianjin 300072, China. Tel.: +86 22 27401940; fax: +86 22 27401940.
*E-mail addresses:* xushg@tju.edu.cn (S. Xu), yfqu@tju.edu.cn (Y. Qu).

0925-8388/$ – see front matter © 2010 Elsevier B.V. All rights reserved.
doi:10.1016/j.jallcom.2010.11.066

**Table 1**
Nominal chemical composition of the specimens.

| Sample | Composition | $E_a$ (eV) |
|---|---|---|
| 0BN | $Ba_{0.68}Sr_{0.32}Ti_{0.99}Sn_{0.01}O_3$ | 1.22 |
| BNM0 | $Ba_{0.68}Sr_{0.308}Bi_{0.006}Na_{0.006}Ti_{0.99}Sn_{0.01}O_3$ | 1.36 |
| BNM5 | $Ba_{0.675}Sr_{0.308}Bi_{0.006}Na_{0.006}Mg_{0.005}Ti_{0.99}Sn_{0.01}O_3$ | 1.31 |
| BNM10 | $Ba_{0.67}Sr_{0.308}Bi_{0.006}Na_{0.006}Mg_{0.010}Ti_{0.99}Sn_{0.01}O_3$ | 1.34 |
| BNM15 | $Ba_{0.665}Sr_{0.308}Bi_{0.006}Na_{0.006}Mg_{0.015}Ti_{0.99}Sn_{0.01}O_3$ | 1.41 |
| BNM20 | $Ba_{0.66}Sr_{0.308}Bi_{0.006}Na_{0.006}Mg_{0.020}Ti_{0.99}Sn_{0.01}O_3$ | 1.25 |
| BNM25 | $Ba_{0.655}Sr_{0.308}Bi_{0.006}Na_{0.006}Mg_{0.025}Ti_{0.99}Sn_{0.01}O_3$ | 1.38 |
| BNM30 | $Ba_{0.65}Sr_{0.308}Bi_{0.006}Na_{0.006}Mg_{0.030}Ti_{0.99}Sn_{0.01}O_3$ | 1.24 |

$$\tan\delta = \frac{fD}{1000} \quad (2)$$

where $C$ and $D$ were the measured capacitance quantities (pF) and loss factors of the samples, respectively. The $h$, $\varphi$, and $f$ were the thickness (cm), diameter (cm) and the testing frequency, respectively. Temperature dependence of dielectric constant and dielectric loss tangent ($\tan\delta$) were obtained with temperature range from −25 °C to 90 °C. The Curie temperature ($T_C$) was determined by the temperature dependence of the dielectric constant. The phase constitution of the samples was analyzed using X-ray diffractometer (XRD; Model GIRAKU D/MAX 2500 V/PC, Japan) with a $2\theta$ range from 20° to 85°. The microstructures of the samples were observed with ESEM (Philip XL 30 ESME), as shown in Fig. 1. When $X > 0.15$, the microstructure homogeneity is improved.

## 3. Results and discussion

### 3.1. XRD measurement of ceramics

Fig. 2(a) shows the XRD patterns of the $(Ba_{0.68}Sr_{0.32})(Ti_{0.99}Sn_{0.01})O_3$ sample and $(Ba_{0.68-x}Sr_{0.308}Bi_{0.006}Na_{0.006}Mg_x)(Ti_{0.99}Sn_{0.01})O_3$ samples with various $X$ values from 0 to 0.030 sintered at 1290–1340 °C for 2 h. The magnesium oxide is failed to detect in all diffraction data. This observation indicates that $Mg^{2+}$ dissolves into the perovskite lattice of $(Ba_{0.68-x}Sr_{0.308}Bi_{0.006}Na_{0.006}Mg_x)(Ti_{0.99}Sn_{0.01})O_3$ ceramics.

As shown in Fig. 2(a), all sintered samples appear to consist of a phase with a cubic perovskite structure. However, Fig. 2(b) clearly reveals that (1 1 1) peaks of BNM0, BNM5 and BNM10 ceramics slightly split. This suggests that the samples of the above are a mixture of cubic (major) and rhombohedral (minor) phases.

The variation of the lattice constant ($a$) for the cubic phase obtained from XRD analysis is plotted in Fig. 3. When $Bi^{3+}$ and $Na^+$ are added into $(Ba_{0.68}Sr_{0.32})(Ti_{0.99}Sn_{0.01})O_3$, the lattice constant ($a$) of BNM0 increases. For $(Ba_{0.68-x}Sr_{0.308}Bi_{0.006}Na_{0.006}Mg_x)(Ti_{0.99}Sn_{0.01})O_3$ system, as $X$ increases, the lattice constant ($a$) of samples decreases when $X \leq 0.020$ and then increases. The observations are supported by diffraction peaks shifting (Fig. 1(b)). The radius of $Bi^{3+}$ (0.96 Å) and $Na^+$ (0.97 Å) is smaller than that of $Sr^{2+}$ (1.16 Å) and $Ba^{2+}$ (1.40 Å) [7,18], so it estimates that the lattice constant ($a$) should decrease when $Bi^{3+}$ and $Na^+$ are introduced into $(Ba_{0.68}Sr_{0.32})(Ti_{0.99}Sn_{0.01})O_3$. But the results obtained from XRD analysis are contrary to the expectation. This may be ascribed to that volatilization of $Bi^{3+}$ and $Na^+$ leads to a lattice defect (mainly $V'''_{Bi}$ and $V'_{Na}$) at sintered temperature. Perhaps the combination of $Bi^{3+}$, $Na^+$ and the lattice defects gives the rhombohedral phase. On the other hand, the radius of $Mg^{2+}$ (0.72 Å) is small and close to the radius of $Ti^{4+}$ (0.61 Å), which could act as an acceptor dopant to replace $Ti^{4+}$ in the B site of $ABO_3$ perovskite structure [19–21].

$$MgO(-TiO_2) \rightarrow Mg''_{Ti} + V_O^{\bullet\bullet} + O_O \quad (3)$$

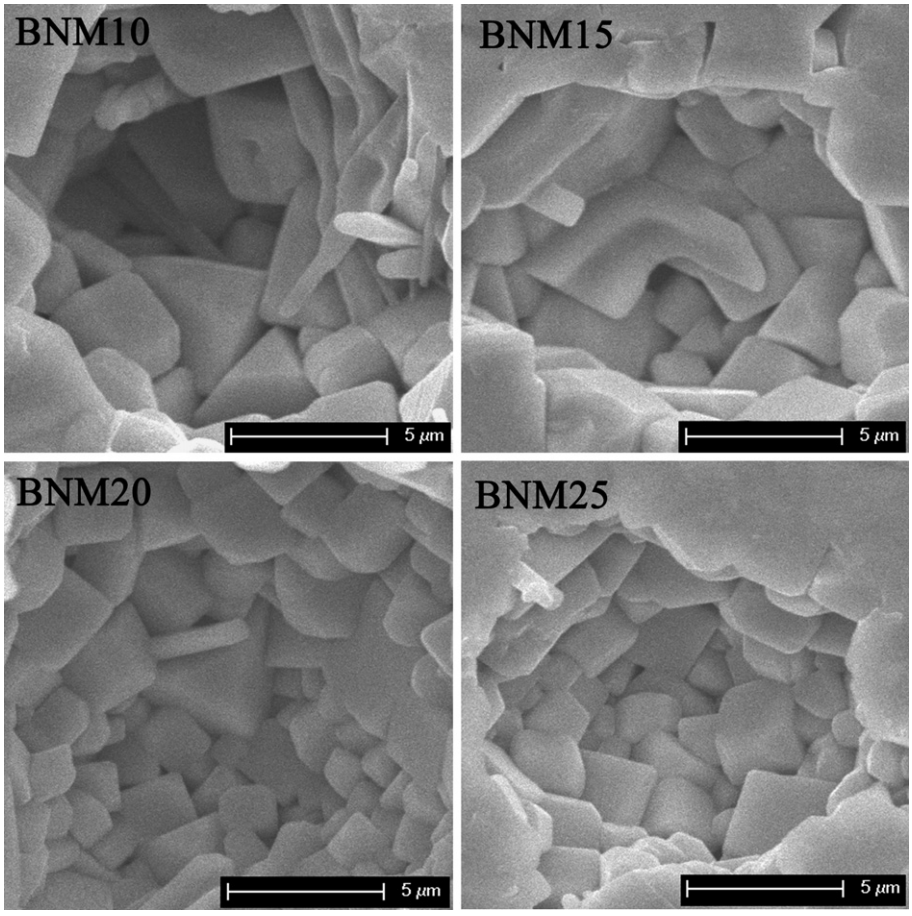


**Fig. 1.** SEM micrographs of the fracture surface of ceramics.

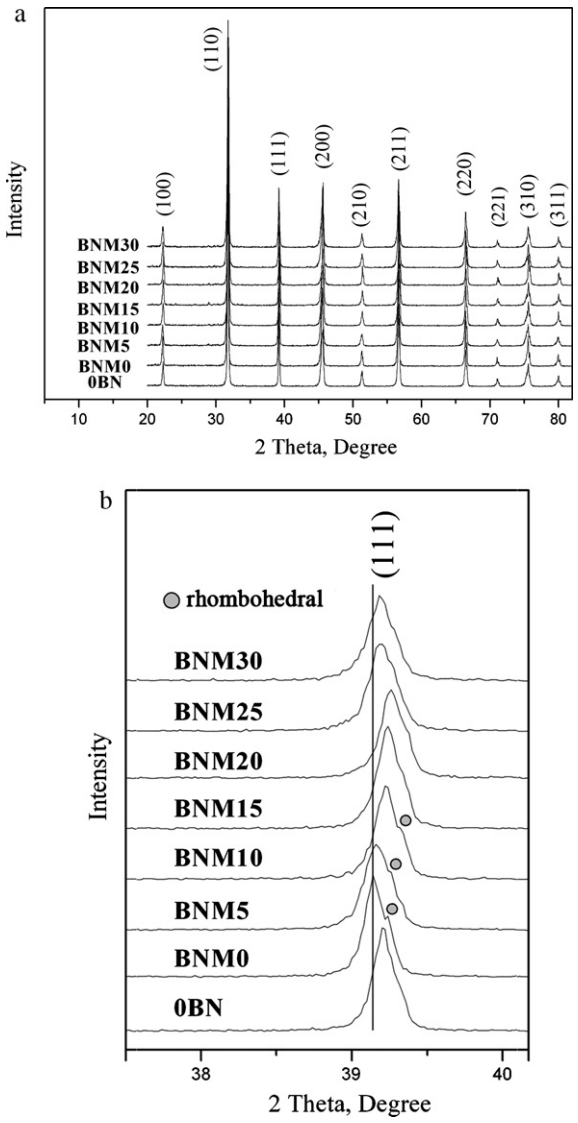


**Fig. 2.** (a) X-ray diffraction of the sintered samples at room temperature and (b) (1 1 1) X-ray diffraction profiles of ceramics at room temperature.

In this paper, the observation suggests that $Mg^{2+}$ occupy in the A site of $ABO_3$ perovskite structure when $X \leq 0.020$ and then replace $Ti^{4+}$ in the B site of $ABO_3$ perovskite structure.

In order to confirm how much for the distortion of the crystal lattice, the parameter $\delta$ is defined by Li and Qu [22].

$$\delta = \frac{\left|(d_{110}(\mathrm{XRD}) - d_{110}(\mathrm{cal})\right|}{d_{110}(\mathrm{XRD})} \quad (4)$$

where $d_{110}$(XRD) and $d_{110}$(cal)denote the face space from XRD test and the face space calculated from Eq. (5), respectively.

$$d_{hkl} = \frac{a}{\sqrt{h^2 + k^2 + l^2}} \quad (5)$$

where $a$ is length of the cell lattice in cubic lattice, $h$, $k$, and $l$ are the index for the crystal face. Fig. 4 shows the variation of the parameter $\delta$ for all samples. It is clear that the curves of the variation of the parameter $\delta$ and the lattice constant ($a$) are similar. In particular, the parameter $\delta$ of BNM0 supports the presence of the lattice defects. As $X$ increases, the parameter $\delta$ of samples decreases when $X \leq 0.020$. This indicates that the addition of $Mg^{2+}$ reduces the lattice defect caused by the volatilization of the $Bi^{3+}$ and $Na^{+}$, and causes the decrease and disappearance of the rhombohedral phase for sam-

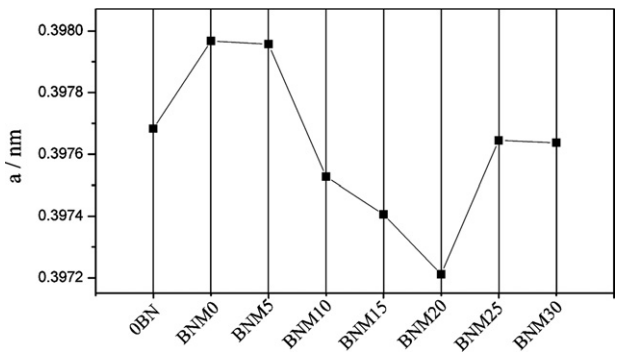


**Fig. 3.** The lattice constant ($a$) of the cubic phase for all ceramics.

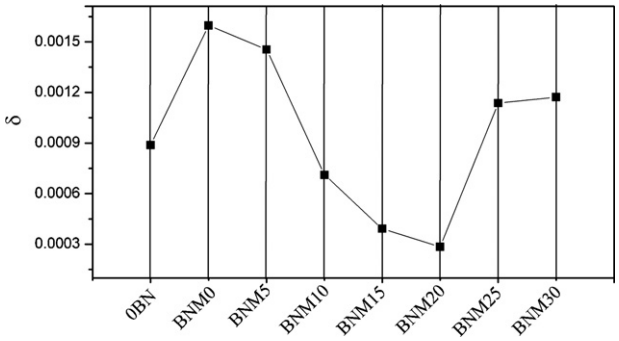


**Fig. 4.** The variation of the parameter $\delta$ for all ceramics.

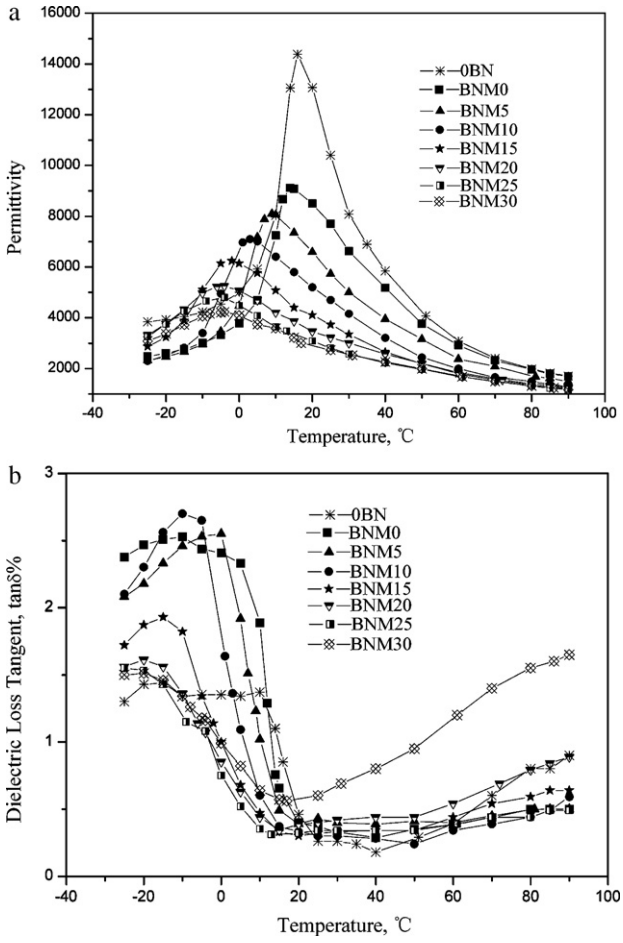


**Fig. 5.** Dielectric properties (at 1 kHz) of samples.

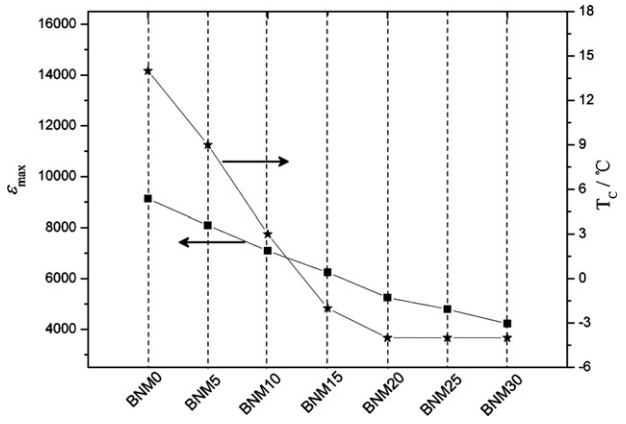


**Fig. 6.** The $\varepsilon_{max}$ and $T_C$ of the specimens as a function of $Mg^{2+}$ content.

ples with $X > 0.010$. While $X > 0.020$, the increase of the parameter $\delta$ suggests the substitution of $Ti^{4+}$ in the B site by $Mg^{2+}$.

### 3.2. Dielectric properties of ceramics

Fig. 5(a) shows the temperature dependence of relative dielectric constant for each sample. It is observed that the Curie peaks ($\varepsilon_{max}$) of samples containing $Bi^{3+}$ and $Na^{+}$ are markedly less than that of 0BN. It is related to the increase of the ionic disorder at the A site of $ABO_3$ perovskite structure. As $X$ value increases from 0 to 0.020, $\varepsilon_{max}$ decreases and $T_C$ shifts to lower temperature, resulting from the occupation of the A site by $Mg^{2+}$, and while $X > 0.020$, $\varepsilon_{max}$ slightly decreases and $T_C$ has no shifts (see Fig. 6), resulting from the replacement of the B site by $Ti^{4+}$ [21].

Fig. 5(b) shows the effects of temperature on dielectric loss of each sample. When $X \leq 0.010$, the dielectric losses in the low tem-

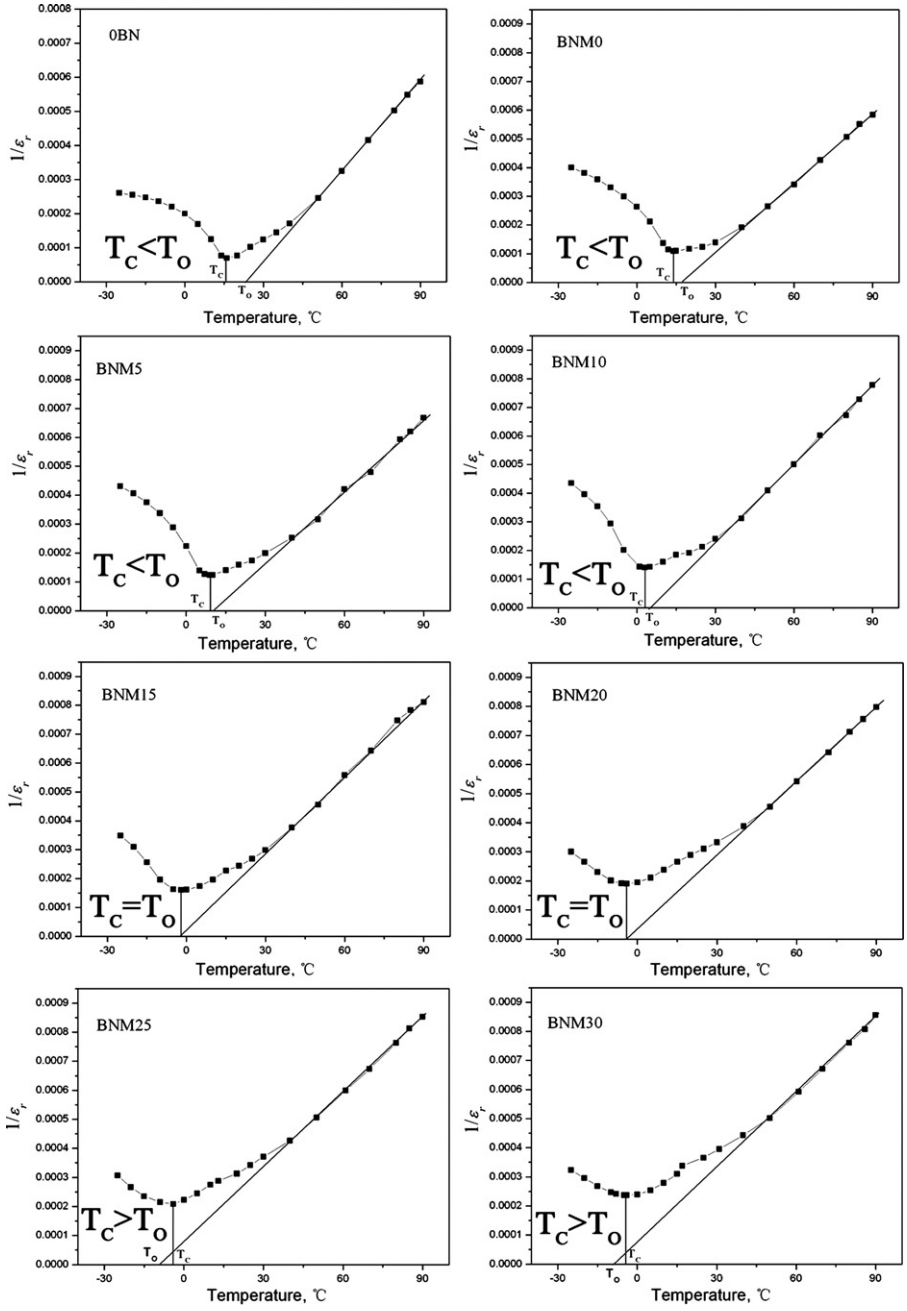


**Fig. 7.** The temperature dependence of $1/\varepsilon_r$ at 1 kHz for all ceramics.

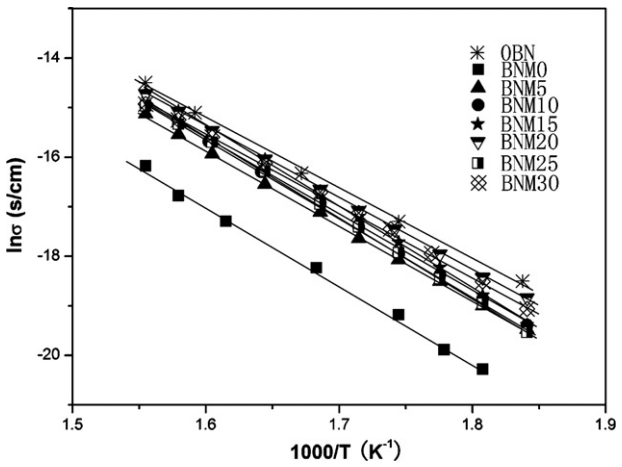


**Fig. 8.** The temperature dependence of conductance for sample.

perature regions significantly increase in comparison with 0BN. As $X > 0.010$, the dielectric losses in the low temperature regions decrease to the value of 0BN. The observation is related to the rhombohedral phase. At lower temperatures, the sintered samples are in ferroelectric region, and the rhombohedral phase is beneficial for the tropism of the ferroelectric domain in additional electric field, so the dielectric losses originated from domain-wall motion increase. When $X > 0.010$, the rhombohedral phase of samples decreases and gradually disappears, and accordingly the dielectric losses in low temperature regions decrease to the value of 0BN. On the other hand, for BNM30, more oxygen vacancies which cause by replacement of $Mg^{2+}$ for $Ti^{4+}$ in B site will result in the larger losses at higher temperatures, as shown in Fig. 5(b).

### 3.3. Phase transition behaviors

In the vicinity of the transition temperature, the dielectric constant $\varepsilon_r$ and Curie temperature $T_C$ corresponding to the dielectric constant peaks ($\varepsilon_{max}$) of the ferroelectric crystals can be described by the Curie–Weiss law:

$$\varepsilon_r = \frac{C}{T - T_0} \tag{6}$$

where $C$ is the Curie constant and $T_0$ is the Curie–Weiss temperature. The ferroelectric–paraelectric phase transition is of first order when $T_0 < T_C$ and of second order when $T_0 = T_C$. Fig. 7 shows the temperature dependence of $1/\varepsilon_r$ at 1 kHz for all sintered samples. In samples 0BN, BNM0, BNM5 and BNM10, it can be seen that the curves of $1/\varepsilon_r$ versus temperature deviate from Curie–Weiss law above the phase transition temperature, which reveal the diffuse phase transition [23]. For $(Ba_{0.68-x}Sr_{0.308}Bi_{0.006}Na_{0.006}Mg_x)(Ti_{0.99}Sn_{0.01})O_3$ system, as $X$ increases, the samples change from the diffuse phase transition to the phase transition of second order, and then to of first order. The comparison and analysis of Figs. 2(b) and 7 imply that the rhombohedral phase appear to play role in the diffuse phase transition for $(Ba_{0.68-x}Sr_{0.308}Bi_{0.006}Na_{0.006}Mg_x)(Ti_{0.99}Sn_{0.01})O_3$ system.

### 3.4. Electric conduction

Fig. 8 shows the temperature dependence of conductance of each sample at DC. According to Arrhenius relationship (Eq. (7)), we fitted each curve and obtained $E_a$ at DC (270–370 °C) for each sample.

$$\sigma = \sigma_0 \exp\left(\frac{-E_a}{kT}\right) \tag{7}$$

where $\sigma_0$ is a pre-exponential factor, $E_a$ is the activation energy and $k$ is the Boltzmann constant. The activation energy values of all samples are shown in Table 1. In the temperature range of 270–370 °C, ceramics are $E_a$ of 1.22–1.41 eV. For pure $BaTiO_3$ ceramics, it is thought that the carriers were formed by lattice inconsistence or defects in grain boundary. Generally, the band gap of $BaTiO_3$ is about 2.5–3.2 eV [24], and the conductivity activation energy of pure $BaTiO_3$ ceramics is about 1.25–1.6 eV. But the activation energy of $V_O^{\cdot\cdot}$ in $SrTiO_3$ is 1.0–1.1 eV, while that in $PbTiO_3$-based materials is 0.9–1.1 eV [25–27]. The analysis of above implies intrinsic conduction dominating the conductivity of all samples in the temperature range 270–370 °C. It is noticed that the conductivity for BNM0 is least, which is connected with the lattice defects ($V'''_{Bi}$ and $V'_{Na}$). Some holes are created under charge neutrality restrictions, which could be described as $V'''_{Bi} + 3h^{\bullet}$ and $V'_{Na} + h^{\bullet}$. These holes neutralize the influence of the electrons. And then the addition of $Mg^{2+}$ reduces $V'''_{Bi}$ and $V'_{Na}$.

## 4. Conclusions

The $(Ba_{0.68-x}Sr_{0.308}Bi_{0.006}Na_{0.006}Mg_x)(Ti_{0.99}Sn_{0.01})O_3$ ceramics were synthesized by solid-state reaction process. The samples ($X \leq 0.010$) are a mixture of cubic (major) and rhombohedral (minor) phases. The rhombohedral phase causes a large dielectric loss in the low temperature regions and plays an important role in the diffuse phase transition of ceramics. While $X > 0.010$, the rhombohedral phase decreases and gradually disappears. The dielectric losses of ceramics in the low temperature regions decrease, and the samples change from the diffuse phase transition to the phase transition of second order, and then to of first order. In the temperature range of 270–370 °C, the intrinsic conduction dominates conductivity of ceramics.

## Acknowledgement

This research is supported by the Production Teaching Research Foundation of Guangdong Province Ministry of Education (Grant No. 2008B090500182).

## References

[1] A. Ioachim, M.I. Toacsan, M.G. Banciu, L. Nedelcu, F. Vasiliu, H.V. Alexandru, C. Berbecaru, G. Stoica, Prog. Solid State Chem. 35 (2007) 513.
[2] Y. Ota, K.I. Kakimoto, H. Ohsato, T. Okawa, J. Eur. Ceram. Soc. 24 (2004) 1755.
[3] Y.C. Chen, P.S. Cheng, C.F. Yang, W.C. Tzou, Ceram. Int. 27 (2001) 809.
[4] H. Zhou, H. Wang, Y. Chen, K. Li, X. Yao, Mater. Chem. Phys. 113 (2009) 1.
[5] R. Zuo, X. Fang, C. Ye, Appl. Phys. Lett. 90 (2007) 092904.
[6] J. Qi, Z. Gui, W. Li, Y. Wang, Y. Wu, L. Li, Mater. Lett. 56 (2002) 507.
[7] J.W. Liou, B.S. Chiou, Mater. Chem. Phys. 51 (1997) 59.
[8] X. Wei, Y. Feng, L. Hang, X. Yao, Ceram. Int. 30 (2004) 1401.
[9] W. Xiaoyong, F. Yujun, Y. Xi, Appl. Phys. Lett. 83 (2003) 2031.
[10] V.V. Shvartsman, W. Kleemann, J. Dec, J. Appl. Phys. 99 (2006) 124111.
[11] S. Lu, Z. Xu, Appl. Phys. Lett. 92 (2008) 232907.
[12] I.A. Souza, L.S. Cavalcante, J.C. Sczancoski, F. Moura, C.O. Paiva-Santos, J.A. Varela, A.Z. Simões, E. Longo, J. Alloys Compd. 477 (2009) 877.
[13] X. Wei, Y. Feng, X. Wan, X. Yao, Ceram. Int. 30 (2004) 1397.
[14] V. Mueller, H. Beige, H.P. Abicht, Appl. Phys. Lett. 84 (2004) 1341.
[15] S.G. Lu, Z.K. Xu, H. Chen, Appl. Phys. Lett. 85 (2004) 5319.
[16] W. Chen, X. Yao, X. Wei, Appl. Phys. Lett. 90 (2007) 182902.
[17] S. Marković, M. Mitrić, N. Cvjetićanin, D. Uskoković, J. Eur. Ceram. Soc. 27 (2007) 505.
[18] D. Lin, K.W. Kwok, H.W.L. Chan, J. Phys. D: Appl. Phys. 40 (2007) 5344.
[19] M.W. Cole, E. Ngo, S. Hirsch, M.B. Okatan, S.P. Alpay, Appl. Phys. Lett. 92 (2008) 072906.
[20] B. Su, T.W. Button, J. Appl. Phys. 95 (2004) 1382.
[21] S. Xu, Y. Qu, C. Zhang, J. Appl. Phys. 106 (2009) 014107.
[22] Y. Li, Y. Qu, Mater. Chem. Phys. 110 (2008) 155.
[23] S.K. Rout, E. Sinha, S. Panigrahi, Mater. Chem. Phys. 101 (2007) 428.
[24] W.D. Kingery, H.K. Bowen, D.R. Uhlmann, Introduction to Ceramics, Wiley-Interscience Publication, 1975.
[25] R. Waser, J. Am. Ceram. Soc. 74 (1991) 1934.
[26] W.L. Warren, K. Vanheusden, D. Dimos, G.E. Pike, B.A. Tuttle, J. Am. Ceram. Soc. 79 (1996) 536.
[27] Y.-Y. Lee, L. Wu, C.-K. Liang, T.S. Wu, Ferroelectrics 138 (1993) 11.